The Astrophysical Journal, 922:14 (9pp), 2021 November 20 https://doi.org/10.3847/1538-4357/ac19ab

Nuclear Physics Multimessenger Astrophysics Constraints on the Neutron Star Equation of State: Adding NICER's PSR J0740+6620 Measurement

Peter T. H. Pang[1,2], Ingo Tews[3], Michael W. Coughlin[4], Mattia Bulla[5], Chris Van Den Broeck[1,2], and Tim Dietrich[6,7]
[1] Nikhef, Science Park 105, 1098 XG Amsterdam, The Netherlands; thopang@nikhef.nl
[2] Institute for Gravitational and Subatomic Physics (GRASP), Utrecht University, Princetonplein 1, 3584 CC Utrecht, The Netherlands
[3] Theoretical Division, Los Alamos National Laboratory, Los Alamos, NM 87545, USA
[4] School of Physics and Astronomy, University of Minnesota, Minneapolis, MN 55455, USA
[5] The Oskar Klein Centre, Department of Astronomy, Stockholm University, AlbaNova, SE-106 91 Stockholm, Sweden
[6] Institut für Physik und Astronomie, Universität Potsdam, Haus 28, Karl-Liebknecht-Str. 24/25, D-14476, Potsdam, Germany
[7] Max Planck Institute for Gravitational Physics (Albert Einstein Institute), Am Mühlenberg 1, Potsdam D-14476, Germany
Received 2021 May 27; revised 2021 July 29; accepted 2021 July 30; published 2021 November 15

Abstract

In the past few years, new observations of neutron stars (NSs) and NS mergers have provided a wealth of data that allow one to constrain the equation of state (EOS) of nuclear matter at densities above nuclear saturation density. However, most observations were based on NSs with masses of about 1.4 $M_\odot$, probing densities up to ∼three to four times the nuclear saturation density. Even higher densities are probed inside massive NSs such as PSR J0740+6620. Very recently, new radio observations provided an update to the mass estimate for PSR J0740+6620, and X-ray observations by the NICER and XMM telescopes constrained its radius. Based on these new measurements, we revisit our previous nuclear physics multimessenger astrophysics constraints and derive updated constraints on the EOS describing the NS interior. By combining astrophysical observations of two radio pulsars, two NICER measurements, the two gravitational-wave detections GW170817 and GW190425, detailed modeling of the kilonova AT 2017gfo, and the gamma-ray burst GRB 170817A, we are able to estimate the radius of a typical 1.4 $M_\odot$ NS to be $11.94^{+0.76}_{-0.87}$ km at 90% confidence. Our analysis allows us to revisit the upper bound on the maximum mass of NSs and disfavors the presence of a strong first-order phase transition from nuclear matter to exotic forms of matter, such as quark matter, inside NSs.

Unified Astronomy Thesaurus concepts: Nuclear physics (2077); Neutron stars (1108); Neutron star cores (1107); Gravitational waves (678)

1. Introduction

One of the major challenges in modern nuclear physics is the characterization of the equation of state (EOS) describing matter at supranuclear densities. These densities are probed inside neutron stars (NSs), which are among the most compact objects in the universe. Therefore, NSs are ideal laboratories to test theories of strong interactions in conditions that cannot be realized experimentally on Earth and to validate or falsify theoretical models for the EOS of dense neutron-rich matter (see, e.g., Lattimer 2012 and Ozel & Freire 2016).

In recent years, a number of new observational constraints on the EOS appeared, either from single NSs, such as the observations of massive pulsars (Demorest et al. 2010; Antoniadis et al. 2013; Arzoumanian et al. 2018; Cromartie et al. 2019) or the X-ray pulse-profile modeling of J0030+0451 by the Neutron-Star Interior Composition Explorer (NICER; Miller et al. 2019b; Riley et al. 2019), or from the observation of binary NS mergers via gravitational waves (GWs) GW170817 (Abbott et al. 2017b, 2018, 2019a, 2019b) and GW190425 (Abbott et al. 2020a, 2021) and the corresponding electromagnetic (EM) counterparts associated with GW signals, namely AT 2017gfo and GRB 170817A (e.g., Arcavi et al. 2017; Coulter et al. 2017; Lipunov et al. 2017; Soares-Santos et al. 2017; Tanvir et al. 2017; Valenti et al. 2017; Abbott et al. 2017a). All of these measurements provide key input to analyze the NS structure and the EOS. This wealth of data made available by multimessenger observations of NSs and NS mergers in recent years has energized the field and triggered many exciting studies (e.g., Bauswein et al. 2017; Metzger 2017; Annala et al. 2018; Most et al. 2018; Radice et al. 2018; Ruiz et al. 2018; Tews et al. 2018b; Capano et al. 2020; Coughlin et al. 2019; Hinderer et al. 2019; Radice & Dai 2019; Dietrich et al. 2020; Raaijmakers et al. 2020; Essick et al. 2020a, 2020b, 2021). However, most of the existing observational data that are sufficiently constraining to improve our understanding of the EOS, e.g., from GW170817 or NICER observations of J0030+0451, probe typical NSs with masses of the order of 1.4 $M_\odot$. Hence, these measurements explore the EOS "only" up to densities of the order of three to four times the nuclear saturation density, $n_{\rm sat} \sim 0.16\,{\rm fm}^{-3}$; see Figure 1. These "intermediate" densities are likely below the onset of a possible phase transition to exotic forms of matter, e.g., quark matter (see, e.g., Annala et al. 2020).

To explore the high-density EOS and place constraints on the possible existence of a phase transition, it is crucial to observe isolated NSs close to the maximum mass supported by the EOS. Alternatively, the high-density part of the EOS can also be probed through binary NS mergers. Once the two stars merge, they can potentially form a hypermassive remnant exceeding even the maximum mass of individual NSs (Margalit & Metzger 2017; Radice et al. 2017; Rezzolla et al. 2018; Ruiz et al. 2018). However, such remnants have not yet been observed through GWs but only through the associated EM observations, which, due to their more involved interpretation, leads to larger uncertainties for the EOS (e.g., Heinzel et al. 2021; Kawaguchi et al. 2020). Fortunately, the recently published second observation by NICER (Wolff et al. 2021; Riley et al. 2021a; Miller et al. 2021b) provides a crucial new data point for an isolated NS close to the maximum mass.

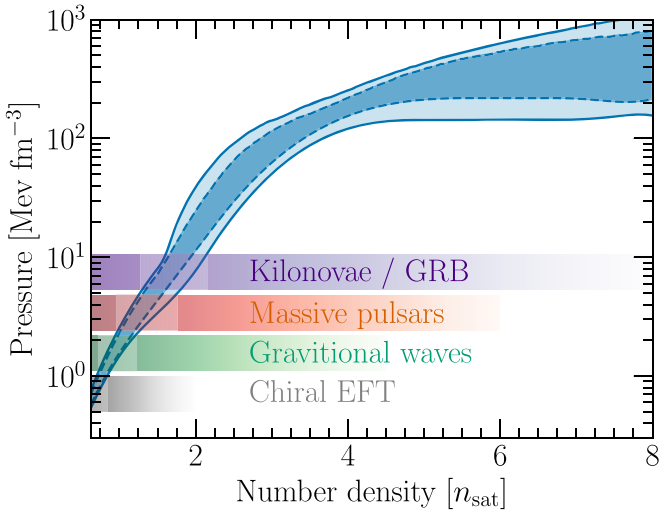

Figure 1. The posterior for the pressure as a function of number density for our final analysis is shown at 68% and 95% credible intervals (light and dark blue shaded bands, respectively). The shaded bars indicate qualitatively which density regions are probed by different NS information, while the corresponding pressures can be extracted using the pressure versus density band. The bars refer to theoretical modeling at low densities using chiral EFT (gray); GWs (green), where the maximum probed density is the central density of GW190425's primary component; massive pulsars (orange), where we give the central density of PSR J0740+6620; and kilonovae and GRBs (purple). Because kilonova and GRB properties depend on the black hole formation mass, and therefore the maximum allowed mass by the EOS, we show the central density of the maximum mass NS.

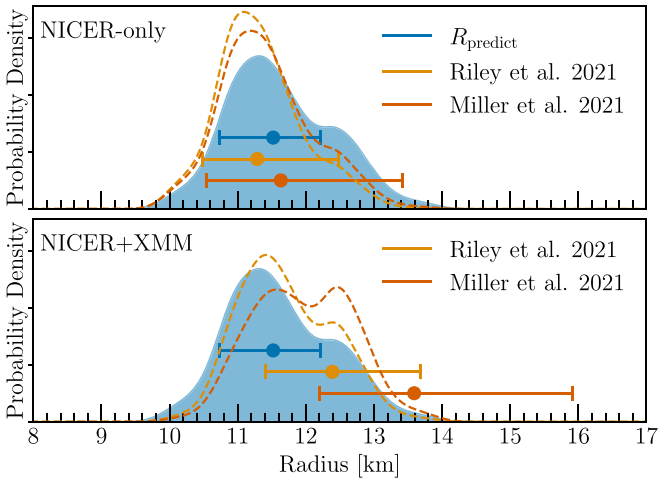

Figure 2. Upper panel: posterior distribution function for $R_{\rm predict}$ from the NMMA framework of Dietrich et al. (2020; blue shaded region). The median and 68% uncertainty for the radius prediction of PSR J0740+6620 are shown as a blue error bar. We also show the NICER-only measurement of Riley et al. (2021a; yellow) and Miller et al. (2021b; red) at 68% uncertainty. The posteriors after the inclusion of the updated observations of PSR J0740+6620 are shown by dashed lines. Lower panel: similar to the upper panel but including XMM data.

NICER is a NASA mission on board the International Space Station that measures the X-ray pulse profile of selected pulsars, which allows one to extract information on the configuration of X-ray hot spots. Additionally, the pulse profile is sensitive to the light bending around the pulsar (see Section 4 in Wolff et al. 2021) and therefore provides information on the NS compactness, which in turn allows one to extract data on the NS mass and radius. The first NICER measurement was reported in 2019 December and targeted the pulsar J0030+0451, for which both mass and radius were unknown. Two independent analyses of the first NICER observation provided mass–radius constraints for this NS of $1.34^{+0.15}_{-0.16} M_\odot$ and $12.71^{+1.14}_{-1.19}$ km (Riley et al. 2019) or $1.44^{+0.15}_{-0.14} M_\odot$ and $13.02^{+1.24}_{-1.06}$ km (Miller et al. 2019b) at 68% confidence.

In its second observation, NICER analyzed X-ray data from the millisecond pulsar PSR J0740+6620 (Riley et al. 2021a; Miller et al. 2021b). This NS is the heaviest NS observed to date, with a known mass of $2.08 \pm 0.07\, M_\odot$ (Fonseca et al. 2021; updated from the original value reported by Cromartie et al. 2019). Combining the known mass with the pulse-profile modeling allowed the NICER collaboration to measure the radius of PSR J0740+6620. Two independent analyses by the NICER collaboration found the radius to be $12.39^{+1.30}_{-0.98}$ (Riley et al. 2021a) and $13.71^{+2.61}_{-1.50}$ (Miller et al. 2021b) km at 68% confidence. While the NICER data provide information about the modulated emission from the star, the analyses of Miller et al. (2021b) and Riley et al. (2021a) additionally used information from the X-ray Multi-Mirror (XMM)-Newton telescope (Struder et al. 2001; Turner et al. 2001) to improve the total flux measurement from the star, due to a smaller rate of background counts.

In this paper, we incorporate the new X-ray observation of PSR J0740+6620 and its updated mass within our existing nuclear physics multimessenger astrophysics (NMMA) framework, which we developed and described in Dietrich et al. (2020). This allows us to revisit our constraints on the NS EOS, in particular the existence of strong first-order phase transitions, the maximum mass of NSs, and the nature of GW190814 (Tews et al. 2021).

This paper is structured as follows. In Section 2, we briefly summarize our previous results and review recent works, including the NICER measurement of PSR J0740+6620. In Section 3, we review our NMMA framework. Using the new NICER data, in Section 4, we discuss our prediction for the NS EOS (Section 4.1), the NS maximum mass, and the probability of GW190814 (Abbott et al. 2020b) being a black hole–NS merger (Section 4.2), and we investigate to what extent the recent NICER observations inform us about the existence of a phase transition in the EOS (Section 4.3). We will give a summary of our results in Section 5.

2. Previous Works

In our previous work (Dietrich et al. 2020), we included the pulsar mass measurements of PSR J0740+6620, PSR J0348+4042, and PSR J1614–2230 (Demorest et al. 2010; Antoniadis et al. 2013; Arzoumanian et al. 2018; Cromartie et al. 2019); GW data from the NS mergers GW170817 and GW190425; information from the kilonova AT 2017gfo and the gamma-ray burst GRB 170817A and its afterglow (Abbott et al. 2017a); and the NICER observation of PSR J0030+0451 (Riley et al. 2019; Miller et al. 2019b) in a Bayesian inference framework based on systematic nuclear physics input from chiral effective field theory (EFT). We obtained a radius of a typical NS of $R_{1.4} = 11.75^{+0.55}_{-0.50}$ km (Dietrich et al. 2020) at 68% uncertainty. Based on these results, our prediction of the radius of PSR J0740+6620 was $R_{\rm predict} = 11.52^{+0.70}_{-0.79}$km at 68% confidence level. We compare this prediction with the recent NICER measurements in Figure 2. We find that our estimate is in excellent agreement with the results obtained in Riley et al. (2021a) and Miller et al. (2021b) using only the

NICER data. Once data from the XMM-Newton observatory are additionally taken into account, the radius is pulled to larger values, decreasing the agreement between our prediction and the measurement, but deviations are $\lesssim 1\sigma$. This effect is stronger for the Maryland–Illinois result (Miller et al. 2021b), which appears to be caused by a number of differences between the individual analyses of Miller et al. (2021b) and Riley et al. (2021a): differences in the prior on the cross-calibration uncertainty of NICER and XMM-Newton, which is allowed to be twice as large as the measured deviation in Miller et al. (2021b) but an order of magnitude larger in the analysis of Riley et al. (2021a); differences in the radius prior, which has an upper bound of 16 km in the analysis of Riley et al. (2021a) and approximately 25 km in Miller et al. (2021b); differences in the sampling algorithms and their convergence that affected the posterior widths; and differences in the assumed distribution of the blank-sky counts to estimate the XMM background.

Since the first announcement of the NICER results for PSR J0740+6620 (NICER 2021), there have been several studies of the implications of this radius measurement (Annala et al. 2021; Biswas 2021; Li et al. 2021; Somasundaram & Margueron 2021). However, these studies did not use the full posterior samples released in Riley et al. (2021a) and Miller et al. (2021b) but employed hard cuts for the radius–mass measurement, which can lead to biases during the final multimessenger analysis, as shown in, e.g., Miller et al. (2019a). In more detail, the studies in Somasundaram & Margueron (2021) and Biswas (2021) were based on phenomenological nuclear physics descriptions but did not include systematic nuclear theory calculations with uncertainty estimates, e.g., from chiral EFT, to constrain the low-density EOS. Instead, Somasundaram & Margueron (2021) studied the impact of the NICER observation of PSR J0740+6620 on the existence of a first-order phase transition or quarkyonic matter using two different models for the high-density part of the EOS. They found that the NICER observation of PSR J0740+6620 cannot rule out first-order phase transitions, but this study also did not systematically include other astrophysical constraints in a Bayesian analysis. Using a different EOS parameterization, Biswas (2021) combined a hypothetical radius measurement of PSR J0740+6620 with previous GW and NICER observations and the recent result for the neutron-skin thickness of ^{208}Pb from the PREX-II experiment (Adhikari et al. 2021). In contrast to these works, Annala et al. (2021) used theoretical nuclear physics input from chiral EFT at low densities and perturbative quantum chromodynamics (QCD) at high densities to constrain the EOS. However, they did not perform a Bayesian analysis to constrain the EOS given available astrophysical data but instead implemented various constraints using hard cuts; see above. None of these papers included multimessenger constraints from a detailed modeling and parameter estimation of EM counterparts associated with binary NS mergers, e.g., from a Bayesian inference of AT 2017gfo and GRB 170817A.

Raaijmakers et al. (2021) and Miller et al. (2021b) were directly based on the NICER and XMM measurements of PSR J0740+6620 and studied the influence of the new NICER data using the full posterior samples. For this purpose, Miller et al. (2021b) employed very general and conservative EOS priors that were not directly informed by nuclear theory calculations at low densities. In addition to the NICER observations of pulsars PSR J0030+0451 and PSR J0740+6620, the final EOS constraints in Miller et al. (2021b) used other heavy-pulsar mass measurements, GW observations of GW170817 and GW190425, and constraints on the nuclear symmetry energy. Results presented in Raaijmakers et al. (2021) were instead constrained by chiral EFT calculations up to $1.1n_{\rm sat}$, comparing four different chiral EFT calculations. In addition, EM information from AT 2017gfo were included, as well as information from GW170817 and GW190425.

In this paper, in contrast to the studies presented in Miller et al. (2021b) and Raaijmakers et al. (2021), we use updated GW models (Dietrich et al. 2019) and different kilonova models with detailed microphysical input that also explore deviations from spherical symmetry (Kasen et al. 2017; Bulla 2019); see Heinzel et al. (2021) and Dietrich et al. (2020) for details about the systematic uncertainties of kilonova modeling. In the case of Miller et al. (2021b), we also include low-density input from chiral EFT.

3. Methodology

Our NMMA framework uses Bayesian inference tools to analyze a set of EOSs with respect to their agreement with several astrophysical observations of NSs.

The initial EOS set is constrained at low densities by calculations of the energy per particle of neutron matter using interactions from chiral EFT (Epelbaum et al. 2009; Machleidt & Entem 2011). Chiral EFT is a low-energy systematic theory for nuclear forces and provides a momentum expansion of two-nucleon and multinucleon interactions. Interactions are arranged in an order-by-order scheme that organizes various interaction mechanisms according to their relative importance. By going to higher orders, the precision of the calculation is improved at the cost of more involved calculations. An important benefit of the chiral EFT scheme is that it allows one to estimate theoretical uncertainties (Epelbaum et al. 2015; Drischler et al. 2020). Given chiral EFT Hamiltonians describing the strong interactions between nucleons, a many-body method is required to solve the many-body Schrödinger equation and calculate the energy per particle. The EOS set used here is constrained by calculations employing quantum Monte Carlo (QMC) methods, which are among the most precise methods to solve the nuclear many-body problem (Carlson et al. 2015) and have been combined with chiral EFT interactions with great success (e.g., Gezerlis et al. 2013; Lonardoni et al. 2018; Piarulli et al. 2018; Lynn et al. 2019). Specifically, here we use the QMC calculations by Tews et al. (2018a) using local chiral EFT interactions from Gezerlis et al. (2013, 2014), Tews et al. (2016), and Lynn et al. (2016), which agree very well with other microscopic calculations based on chiral EFT (Huth et al. 2021). Furthermore, Raaijmakers et al. (2021) showed that EOS constraints are only weakly dependent on the choice of a particular chiral EFT calculation at low densities.

The range of applicability of chiral EFT calculations is limited because the average nucleon momentum increases with density and the momentum expansion breaks down. While the exact breakdown density for individual chiral EFT interactions is unknown, it was estimated to be between 1 and $2n_{\rm sat}$ for the QMC calculations used here (Tews et al. 2018a; Essick et al. 2020b). We constrain the NS EOS with QMC calculations of the EOS up to a density of $1.5n_{\rm sat}$, but the results were found to show only a very weak dependence on a variation of this density between 1 and $2n_{\rm sat}$ (Essick et al. 2020b). We use the speed-of-sound extension scheme from Tews et al. (2018b) to extend the EOS to higher densities in a general way. The speed-of-sound extension scheme allows us to explore the

Table 1
Summary of the Resulting Posteriors for the Radius of a Typical NS $R_{1.4}$, the NS Maximum Mass $M_{\rm max}$, and the Bayes Factor for Phase Transition against Its Absence, $\mathcal{B}^{\rm PT}_{\rm NPT}$

Quantity	NMMA	NMMA + Miller et al. (2021b)	NMMA + Riley et al. (2021a)	NMMA + Combined Miller et al. (2021b) & Riley et al. (2021a)
$R_{1.4}$	$11.75^{+0.86}_{-0.81}$km	$11.62^{+0.85}_{-0.79}$ km($12.03^{+0.77}_{-0.87}$ km)	$11.56^{+0.79}_{-0.76}$ km($11.84^{+0.79}_{-0.80}$ km)	$11.59^{+0.83}_{-0.76}$ km($11.94^{+0.76}_{-0.87}$ km)
$M_{\rm max}$	$2.18^{+0.14}_{-0.13}M_\odot$	$2.16^{+0.15}_{-0.12}M_\odot$($2.18^{+0.15}_{-0.15}M_\odot$)	$2.15^{+0.14}_{-0.12}M_\odot$($2.17^{+0.15}_{-0.13}M_\odot$)	$2.15^{+0.15}_{-0.12}M_\odot$($2.18^{+0.16}_{-0.13}M_\odot$)
$\mathcal{B}^{\rm PT}_{\rm NPT}$	0.27 ±0.01	0.29 ± 0.01 (0.21 ± 0.01)	0.30 ± 0.01 (0.23 ± 0.01)	0.29 ± 0.01 (0.23 ± 0.01)

Note. The values shown outside (inside) parentheses refer to the results without (with) inclusion of XMM data. All quoted errors are given at a 90% credible interval.

physically plausible EOS space without making any strong model assumptions (see also Greif et al. 2019 and Raaijmakers et al. 2021). We only require the EOSs to explore speeds of sound, c_S, limited by $0 \leqslant c_S \leqslant 1$ in units of the speed of light, and provide a maximum mass for NSs of at least 1.9 $M_\odot$. Our EOS set explicitly includes EOS with regions of sudden stiffening or softening, e.g., strong first-order phase transitions toward exotic forms of matter. For our EOS set, we impose a uniform prior on the radius of a typical 1.4 $M_\odot$ NS, $R_{1.4}$. To estimate the impact of the particular choice of the EOS prior, we have also investigated an EOS prior without this additional requirement; see Table 2 of the Appendix.

As a next step, we analyze our EOS set with respect to available NS observations. We start by incorporating a constraint on the maximum mass of NSs through the radio observations of the heaviest pulsars known to date, PSR J0348+4042 (Antoniadis et al. 2013) and PSR J1614–2230 (Arzoumanian et al. 2018). The existence of these pulsars can only be explained if the NS EOS supports masses that lie above the individual masses of these pulsars. Hence, radio pulsar measurements of heavy NSs provide a lower bound on the maximum NS mass and the constraints of the high-density EOS; see Figure 1. We stress that at this stage, we do not include the mass measurement of PSR J0740+6620, because information will be included through the new NICER measurement. An upper bound of the maximum NS mass follows from the EM observation of GRB 170817A and AT 2017gfo. As outlined in, e.g., Margalit & Metzger (2017), the observed EM signatures indicate the formation of a black hole as the final product of the binary NS merger GW170817. Combining this information with the estimated total remnant mass from the GW observation leads to a nonrotating maximum NS mass of $M_{\rm max} \leqslant 2.16^{+0.17}_{-0.15}M_\odot$ (Rezzolla et al. 2018). Incorporating the constraints on the maximum mass leads to a reweighting of the original chiral EFT EOS set.

As a next step, we include the NICER measurement of PSR J0030+0451, for which the inferred mass–radius posterior probability distributions were not dominated by systematic uncertainties and inferred system parameters were in agreement for different analyses (Riley et al. 2019; Miller et al. 2019b). Finally, we use the resulting EOS set for GW and kilonova parameter estimation following the methods outlined in Dietrich et al. (2020).

We now include the NICER observations of PSR J0740+6620 (Riley et al. 2021a; Miller et al. 2021b), which are based on a Bayesian inference approach to analyze the energy-dependent thermal X-ray signal of PSR J0740+6620. We employ the posterior samples obtained with the two circular, uniform-temperature spot models from Miller et al. (2021a, 2021b) and the two disjoint, uniform-temperature spots model from Riley et al. (2021a, 2021b). These models provide the best agreement with the observed NICER and NICER+XMM data and, for the latter, constrain the radius of PSR J0740+6620 with a mass of $2.08 \pm 0.07\,M_\odot$ (Cromartie et al. 2019; Fonseca et al. 2021) to $13.71^{+2.61}_{-1.50}$ km and $12.39^{+1.30}_{-0.98}$ km at 68% confidence for Miller et al. (2021b) and Riley et al. (2021a), respectively.

The corresponding likelihood $\mathcal{L}_{\rm NICER}$ is given by

$$\begin{aligned}\mathcal{L}_{\rm NICER}({\rm EOS}) &= \int dMdR\; p_{\rm NICER}(M, R)\pi(M, R|{\rm EOS}) \\ &\propto \int dMdR\; p_{\rm NICER}(M, R)\delta(R - R(M, {\rm EOS})) \\ &\propto \int dM\; p_{\rm NICER}(M, R = R(M, {\rm EOS})), \end{aligned} \quad (1)$$

where $p_{\rm NICER}(M, R)$ is the joint-posterior probability distribution of the mass and radius of PSR J0740+6620 as measured by NICER, and we use the fact that the radius is a function of mass for a given EOS.

4. Results

In the following, we discuss the results of our NMMA framework when the new NICER measurement is included. We give results using constraints from the X-PSI analysis by the Amsterdam group (Riley et al. 2021a) or the analysis of the Illinois–Maryland group (Miller et al. 2021b) outside/inside parentheses. The combined results refer to an analysis using the average of the two (M, R) posterior distributions for PSR J0740+6620. Our findings are summarized in Table 1.

4.1. Neutron Star Equation of State

In Figure 3, we show the EOS and mass–radius posteriors after the inclusion of the radius measurement of PSR J0740+6620 using only NICER data. In this case, the NICER radius measurement shows excellent agreement with the NMMA prediction for the radius of PSR J0740+6620; see also Figure 2. Because the NICER-only data slightly prefer a softer EOS in the NMMA set, we observe a softening of our total EOS posterior. This can also be seen from the posteriors for the mass–radius relation, which is slightly shifted to lower radii. For example, the NMMA framework predicts the radius of a 1.4 $M_\odot$ NS, $R_{1.4}$, to be $11.75^{+0.86}_{-0.81}$km without the new NICER measurement. Including the measurement, we find $11.56^{+0.79}_{-0.76}$ km($11.62^{+0.85}_{-0.79}$ km) and a combined result of $11.59^{+0.83}_{-0.76}$ km at 90% credibility. The median predictions change minimally, by ∼200 m, and the uncertainties improve slightly from 4.5% to 4.2% for the combined result at a 68% credible interval (and from 7.1% to 6.9% at a 90% credible interval). Similarly, the radius posteriors of PSR J0740+6620

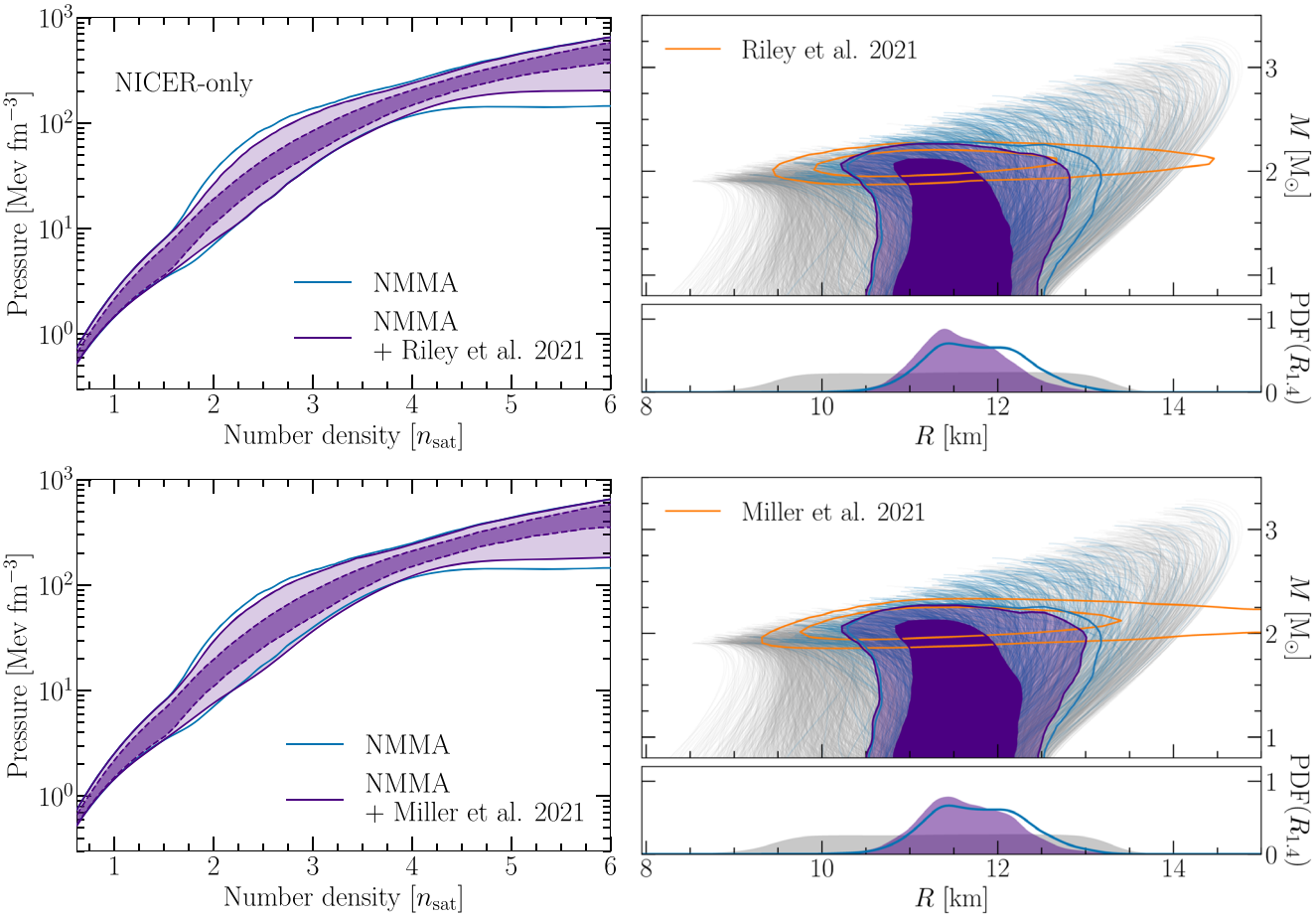

Figure 3. Left panels: posterior for the pressure as a function of number density including the NICER-only observations of PSR J0740+6620 from Riley et al. (2021a; upper panel) and Miller et al. (2021b; lower panel). The bands indicate 68% and 95% credible intervals. The 95% band for the NMMA result without the new NICER measurement is shown as a comparison (blue line). Right panels: NICER mass–radius posteriors of PSR J0740+6620 plotted at 68% and 95% confidence intervals (orange contours) and the EOSs included in the analysis (gray lines). The 95% contour for the NMMA result without including the new NICER observation is shown as a thick blue line, while the individual EOSs within this credible interval of the NMMA analysis are shown as thin blue lines. The resulting mass–radius posterior after the inclusion of the new NICER-only observation is shown in purple for the NICER results of Riley et al. (2021a; upper panel) and Miller et al. (2021b; lower panel) at 68% and 95% credible intervals. The 1D insets show the posteriors for $R_{1.4}$ with (purple) and without (blue) the inclusion of the NICER-only measurement of PSR J0740+6620.

after including the NICER-only data are shown in Figure 2. The estimated radius changes from $11.52^{+0.70}_{-0.79}$ to $11.26^{+0.56}_{-0.63}$km ($11.35^{+0.61}_{-0.72}$km) at 68% credibility.

The situation is different when the XMM data are added. In Figure 4, we show our results for the EOS and the mass–radius relation when including the NICER and XMM data. Now these measurements predict larger radii compared to our initial estimation for PSR J0740+6620; see Figure 2. This slightly shifts our EOS posterior to the stiffer end and the mass–radius relation to larger radii. By including the NICER-XMM measurement, $R_{1.4}$ changes from $11.75^{+0.86}_{-0.81}$km without the new data to $11.84^{+0.79}_{-0.80}$ km($12.03^{+0.77}_{-0.87}$ km) and a combined result of $11.94^{+0.76}_{-0.87}$ km. Though the measured radii are well above the NMMA prediction, the uncertainties are sizable; hence, the radius measurement of PSR J0740+6620 does not change our EOS results significantly. The medians shift to slightly larger values but remain statistically consistent with a comparable uncertainty. Similarly, the NMMA radius prediction for PSR J0740+6620 changes from $11.52^{+0.70}_{-0.79}$km without the new data to $11.63^{+0.66}_{-0.79}$km ($11.96^{+0.80}_{-0.75}$km) at 68% credibility.

4.2. NS Maximum Mass and GW190814

The radius measurement of PSR J0740+6620 and its impact on the EOS allow us to revisit our estimate for the maximum allowed mass for NSs, $M_{\rm max}$, which we found to be $M_{\rm max} = 2.18^{+0.14}_{-0.13}M_\odot$ without including the new NICER data (Tews et al. 2021); see Figure 5. Please note that this original estimate used the previously larger mass for PSR J0740+6620 from Cromartie et al. (2019), which was updated to a lower value in Fonseca et al. (2021).

Because the NICER-only data favor a slightly softer EOS (see the previous discussion), the maximum mass estimate decreases slightly to $M_{\rm max} = 2.15^{+0.14}_{-0.12}M_\odot$($2.16^{+0.15}_{-0.12}M_\odot$). When additionally considering the XMM data, the new data prefer a slightly stiffer EOS, but the maximum mass estimate, $2.17^{+0.15}_{-0.13}M_\odot$($2.18^{+0.15}_{-0.15}M_\odot$), does not change significantly. The reason is that the upper limit on $M_{\rm max}$ is mainly determined by the constraint of Rezzolla et al. (2018). Because of the strong impact of this constraint, we also consider the scenario where this upper limit on $M_{\rm max}$ is not included. In this case, $M_{\rm max}$ is found to be $2.34^{+0.34}_{-0.28}M_\odot$ without the new NICER data and

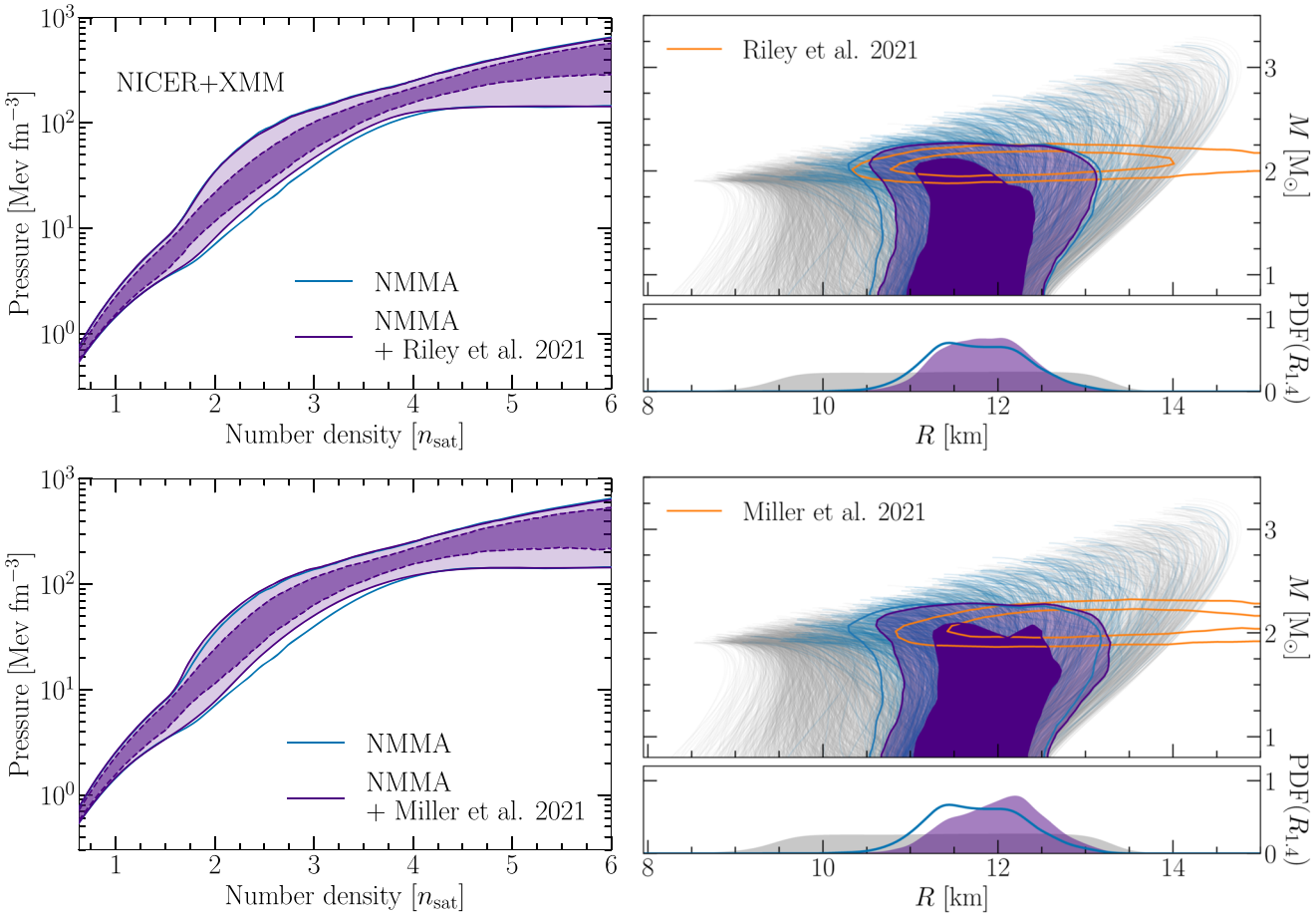

Figure 4. Same as Figure 3 but using the NICER+XMM data.

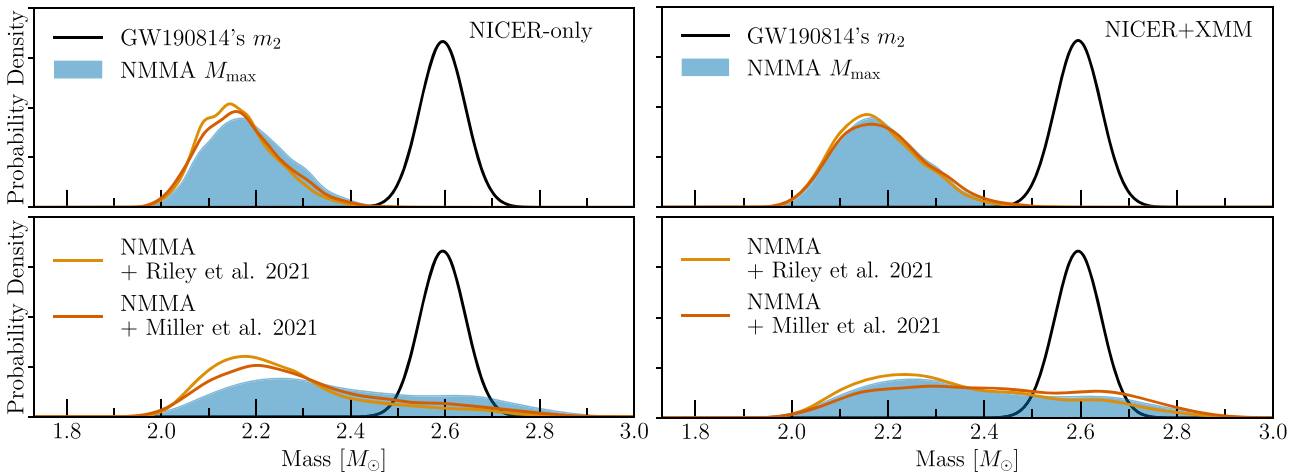

Figure 5. Distributions of $M_{\rm max}$ without the new NICER observation (blue bands) and when including the posterior from Riley et al. (2021a; yellow lines) and Miller et al. (2021b; red lines). We show results for the NICER-only data (left panels) and the NICER+XMM data (right panels) and including the $M_{\rm max}$ upper limit suggested in Rezzolla et al. (2018; upper panels) and when this upper limit on $M_{\rm max}$ is relaxed (lower panels).

changes to $2.23^{+0.31}_{-0.20}M_\odot$ ($2.26^{+0.36}_{-0.24}M_\odot$) including the NICER-only data and $2.31^{+0.37}_{-0.25}M_\odot$ ($2.40^{+0.35}_{-0.32}M_\odot$) for the NICER and XMM data. The changes are small because the increased stiffness coming from the pulsar radius measurement competes with the updated lower pulsar mass.

The posterior of $M_{\rm max}$ affects the classification of the secondary component of GW190814 (Abbott et al. 2020b), where a 2.6 $M_\odot$ compact object merged with a 22 $M_\odot$ black hole. Due to its extreme mass ratio and the low primary spin, the nature of the secondary component cannot be extracted from observational data. Instead, it has to be extracted from EOS modeling; see, e.g., Kalogera & Baym (1996), Biswas et al. (2021), Essick & Landry (2020), and Tews et al. (2021). To examine the probability of the secondary component of GW190814 being an NS, the posterior

Table 2
Summary of the Resulting Posteriors without a Uniform Prior on $R_{1.4}$ Imposed for the Radius of a Typical NS $R_{1.4}$, the NS Maximum Mass $M_{\rm max}$, and the Bayes Factor for Phase Transition against Its Absence, $\mathcal{B}^{\rm PT}_{\rm NPT}$

Quantity	NMMA	NMMA + Miller et al. (2021b)	NMMA + Riley et al. (2021a)	NMMA + Combined Miller et al. (2021b) & Riley et al. (2021a)
$R_{1.4}$	$11.94^{+0.58}_{-0.64}$km	$11.86^{+0.58}_{-0.58}$km($12.04^{+0.61}_{-0.61}$km)	$11.82^{+0.56}_{-0.57}$km($11.96^{+0.62}_{-0.57}$km)	$11.84^{+0.56}_{-0.59}$km($12.00^{+0.61}_{-0.60}$km)
$M_{\rm max}$	$2.19^{+0.14}_{-0.13}M_\odot$	$2.18^{+0.15}_{-0.12}M_\odot$($2.18^{+0.18}_{-0.13}M_\odot$)	$2.17^{+0.15}_{-0.11}M_\odot$($2.17^{+0.16}_{-0.12}M_\odot$)	$2.18^{+0.14}_{-0.12}M_\odot$($2.18^{+0.17}_{-0.13}M_\odot$)
$\mathcal{B}^{\rm PT}_{\rm NPT}$	0.64 ± 0.01	0.62 ± 0.01 (0.67 ± 0.01)	0.60 ± 0.01 (0.64 ± 0.01)	0.61 ± 0.01 (0.65 ± 0.01)

Note. The values shown outside (inside) parentheses refer to the results without (with) inclusion of XMM data. All quoted errors are given at a 90% credible interval.

of $M_{\rm max}$, $p_{M_{\rm max}}(m)$, and that of GW190814's m_2, $p_{m_2}(m)$, are compared. The probability of GW190814 being an NS–black hole merger is given by (Tews et al. 2021)

$$P(\text{GW190814 is NSBH}) = \int_0^\infty d\Delta m \int_{-\infty}^{\infty} dm\, p_{M_{\rm max}}(m+\Delta m) p_{m_2}(m). \quad (2)$$

Due to the strong tension between GW190814's m_2 and the upper limit from Rezzolla et al. (2018), the inclusion of the NICER measurement of PSR J0740+6620 does not impact the classification of this system. With or without the new NICER measurement, the probability of GW190814 being an NS–black hole merger is estimated to be <0.1%. However, if we relax the upper limit on $M_{\rm max}$, i.e., do not include the analysis of Rezzolla et al. (2018), the probabilities change. Using the NICER-only data, the probability of GW190814 being an NS–black hole system changes to 6.30% (10.5%), lower than the previous estimation of 19% in Tews et al. (2021). When additionally including XMM data, the probability of GW190814 being an NS–black hole system changes to 15.2% (24.4%). The corresponding posterior distributions are shown in Figure 5. Given all current observational and theoretical knowledge of the NS EOS, a binary black hole merger remains the most consistent scenario for GW190814.

4.3. Existence of a Phase Transition

It is predicted by QCD that nucleonic matter undergoes a phase transition to quark matter at very high densities. If such a phase transition is realized in NSs, at which exact density such a phase transition would occur and which properties this phase transition would exhibit are unknown (Glendenning 1992; Alford 2002; Alford et al. 2007). A strong first-order phase transition, i.e., a segment in the EOS where the speed of sound vanishes, would be a "smoking-gun" signature for the existence of exotic forms of matter inside NSs.

Here we calculate the Bayes factor $\mathcal{B}^{\rm PT}_{\rm NPT}$ for the presence of such a strong first-order phase transition against the absence of it. The Bayes factor $\mathcal{B}^{\rm PT}_{\rm NPT}$ is given by

$$\mathcal{B}^{\rm PT}_{\rm NPT} \equiv \frac{P(d|\mathcal{H}_{\rm PT})}{P(d|\mathcal{H}_{\rm NPT})} = \frac{P(\mathcal{H}_{\rm PT}|d)}{P(\mathcal{H}_{\rm NPT}|d)} \Big/ \frac{P(\mathcal{H}_{\rm PT})}{P(\mathcal{H}_{\rm NPT})}, \quad (3)$$

where $P(\mathcal{H}_{\rm PT}|d)$ ($P(\mathcal{H}_{\rm NPT}|d)$) is the posterior probability for the presence (absence) of a phase transition, and $P(\mathcal{H}_{\rm PT})$ ($P(\mathcal{H}_{\rm NPT})$) is the corresponding prior probability. A Bayes factor larger than 1 indicates that the presence of a phase transition is preferred, while a Bayes factor smaller than 1 suggests that the presence of a phase transition is disfavored. Without information from the NICER measurement of PSR J0740+6620, we find the Bayes factor to be 0.27 ± 0.01.

When including NICER-only data, softer EOSs are preferred, and the Bayes factors in favor of a phase transition change to 0.30 ± 0.01 (0.29 ± 0.01). In this case, the NICER radius measurement of PSR J0740+6620 alone slightly increases the Bayes factor for the presence of a strong first-order phase transition within an NS with respect to the original NMMA analysis, but such a transition remains disfavored considering all data. On the other hand, with the additional inclusion of the XMM data, the Bayes factor changes to 0.23 ± 0.01 (0.21 ± 0.01). Following the interpretation of the Bayes factor described in Jeffreys (1961), the presence of a phase transition inside an NS is disfavored in all cases, yet it is not ruled out, in agreement with the findings of Somasundaram & Margueron (2021).

In all cases, even though a radius measurement of PSR J0740+6620 probes the EOS at the highest densities we can observe in the cosmos to date, the NICER data add only limited information due to their sizable uncertainties. In addition, it remains inconclusive if the radius measurement of PSR J0740+6620 itself suggests the presence of a phase transition inside an NS because the NICER-only and NICER-XMM data shift the Bayes factors in different directions; see the last column in Table 1. Moreover, an analysis using a different EOS prior shows that the direction of the shift is prior-dependent; see Table 2.

5. Summary

Using our NMMA framework (Dietrich et al. 2020), we have studied the impact of the new NICER observations of PSR J0740+6620 on the NS EOS. While the NICER data alone show good agreement with our previous NMMA predictions and therefore validate our results, the additional inclusion of XMM data prefers a slightly stiffer EOS. However, due to the large uncertainties of 10%–20% in the NICER radius measurement of PSR J0740+6620, the changes remain small.

In particular, the radius of a 1.4 $M_\odot$ NS $R_{1.4}$ changes from $R_{1.4} = 11.75^{+0.86}_{-0.81}$ km (Dietrich et al. 2020) to $11.56^{+0.79}_{-0.76}$ and $11.62^{+0.85}_{-0.79}$ km for the analyses from Riley et al. (2021a) and Miller et al. (2021b), respectively, at 90% confidence without the XMM data and $11.84^{+0.79}_{-0.80}$ and $12.03^{+0.77}_{-0.87}$ km with the XMM data. Combining the latter results, we obtain a final radius estimate of $11.94^{+0.76}_{-0.87}$ km (at 90% confidence), showing excellent agreement with our initial prediction. Although the NICER-XMM data are informative, their large measurement uncertainties prevent them from significantly influencing our NMMA analysis.

We also investigated the impact of including the NICER observation on PSR J0740+6220 on the maximum allowed NS mass, $M_{\rm max}$, and its influence on the probability of GW190814 being an NS–black hole merger. The upper limit on the maximum mass is mainly influenced by EM observations of GW170817 (Margalit & Metzger 2017; Rezzolla et al. 2018); therefore, the NICER data do not result in an observable impact. When not enforcing this upper bound on $M_{\rm max}$, the probability of GW190814 being an NS–black hole merger changes from 19% to 6.3% and 10.5% (15.2% and 24.4%) with the inclusion of NICER (NICER+XMM) data from Riley et al. (2021a) and Miller et al. (2021b), respectively. Based on these estimations, it remains most plausible that GW190814 originated from a binary black hole merger.

Finally, we studied the possibility for a first-order phase transition to be present inside NSs. Following the interpretation of Bayes factors suggested in Jeffreys (1961), the presence of a phase transition inside NSs is disfavored, yet it is not ruled out. However, this result is mainly impacted by previous multi-messenger observations of NSs, and the impact of the new NICER measurement is small.

Observations of NSs have the potential to help us answer key questions in nuclear physics, but current uncertainties in individual data remain large. This highlights the importance of flexible multimessenger frameworks that can use input from nuclear theory modeling of the EOS, laboratory experiments, and complementary observations of NSs to probe different aspects and paint a complete picture of the EOS.

We thank LIGO's extreme matter group for valuable comments and discussions. We are also grateful to the NICER collaboration for releasing their posterior samples and collected data. P.T.H.P. and C.V.D.B. are supported by the research program of the Netherlands Organization for Scientific Research (NWO). The work of I.T. was supported by the U.S. Department of Energy, Office of Science, Office of Nuclear Physics, under contract No. DE-AC52-06NA25396; the Laboratory Directed Research and Development program of Los Alamos National Laboratory under project Nos. 20190617PRD1 and 20190021DR; and the U.S. Department of Energy, Office of Science, Office of Advanced Scientific Computing Research, Scientific Discovery through Advanced Computing (SciDAC) program. M.W.C. acknowledges support from the National Science Foundation with grant No. PHY-2010970. M.B. acknowledges support from the Swedish Research Council (Reg. No. 2020-03330). Computations were performed on the national supercomputer Hawk at the High Performance Computing Center Stuttgart (HLRS) under grant No. 44189 and the SuperMUC-NG at Leibniz Supercomputing Centre Munich under project No. pn29ba. Computational resources have also been provided by the Los Alamos National Laboratory Institutional Computing Program, which is supported by the U.S. Department of Energy National Nuclear Security Administration under contract No. 89233218CNA000001, and by the National Energy Research Scientific Computing Center (NERSC), which is supported by the U.S. Department of Energy, Office of Science, under contract No. DE-AC02-05CH11231. This research has made use of data, software, and/or web tools obtained from the Gravitational Wave Open Science Center (https://www.gw-openscience.org), a service of the LIGO Laboratory, the LIGO Scientific Collaboration, and the Virgo Collaboration. LIGO is funded by the U.S. National Science Foundation. Virgo is funded by the French Centre National de Recherche Scientifique (CNRS), the Italian Istituto Nazionale della Fisica Nucleare (INFN), and the Dutch Nikhef, with contributions by Polish and Hungarian institutes.

Appendix
Impact of EOS Prior

In Table 2, we present a summary of the resulting posteriors for the quantities of interest using an EOS prior that is not uniform in $R_{1.4}$, i.e., a prior that is "natural" to our speed-of-sound extension scheme. The posteriors on $R_{1.4}$ and $M_{\rm max}$ are consistent with the results shown in Table 1 within the uncertainties.

In contrast, the Bayes factors $\mathcal{B}^{\rm PT}_{\rm NPT}$ are prior-sensitive, and their values shift significantly from the results in Table 1. Because the nonuniform prior set does not explore as many EOSs with phase transitions as the uniform $R_{1.4}$ prior set, the shifts of the Bayes factors change. However, the presence of a phase transition inside an NS is still disfavored in all cases but cannot be ruled out.

ORCID iDs

Peter T. H. Pang https://orcid.org/0000-0001-7041-3239
Ingo Tews https://orcid.org/0000-0003-2656-6355
Michael W. Coughlin https://orcid.org/0000-0002-8262-2924
Mattia Bulla https://orcid.org/0000-0002-8255-5127
Chris Van Den Broeck https://orcid.org/0000-0001-6800-4006
Tim Dietrich https://orcid.org/0000-0003-2374-307X

References

Abbott, B., et al. 2017a, ApJL, 848, L12
Abbott, B., et al. 2020a, ApJL, 892, L3
Abbott, B. P., et al. 2017b, PhRvL, 119, 161101
Abbott, B. P., et al. 2018, PhRvL, 121, 161101
Abbott, B. P., et al. 2019a, PhRv, X9, 031040
Abbott, B. P., et al. 2019b, PhRv, X9, 011001
Abbott, R., et al. 2020b, ApJ, 896, L44
Abbott, R., et al. 2021, PhRvX, 11, 021053
Adhikari, D., et al. 2021, PhRvL, 126, 172502
Alford, M. 2002, eConf, C010815, 137
Alford, M., Blaschke, D., Drago, A., et al. 2007, Natur, 445, E7
Annala, E., Gorda, T., Katerini, E., et al. 2021, arXiv:2105.05132
Annala, E., Gorda, T., Kurkela, A., Nättilä, J., & Vuorinen, A. 2020, NatPh, 16, 907
Annala, E., Gorda, T., Kurkela, A., & Vuorinen, A. 2018, PhRvL, 120, 172703
Antoniadis, J., Freire, P. C., Wex, N., et al. 2013, Sci, 340, 6131
Arcavi, I., et al. 2017, Natur, 551, 64
Arzoumanian, Z., et al. 2018, ApJS, 235, 37
Bauswein, A., Just, O., Janka, H.-T., & Stergioulas, N. 2017, ApJ, 850, L34
Biswas, B. 2021, arXiv:2105.02886
Biswas, B., Nandi, R., Char, P., Bose, S., & Stergioulas, N. 2021, MNRAS, 505, 1600
Bulla, M. 2019, MNRAS, 489, 5037
Capano, C. D., Tews, I., Brown, S. M., et al. 2020, NatAs, 4, 625
Carlson, J., Gandolfi, S., Pederiva, F., et al. 2015, RvMP, 87, 1067
Coughlin, M. W., Dietrich, T., Margalit, B., & Metzger, B. D. 2019, MNRAS: Letters, 489, L91
Coulter, D. A., et al. 2017, Sci, 358, 1556
Cromartie, H. T., et al. 2019, NatAs, 4, 72
Demorest, P., Pennucci, T., Ransom, S., Roberts, M., & Hessels, J. 2010, Natur, 467, 1081
Dietrich, T., Coughlin, M. W., Pang, P. T. H., et al. 2020, Sci, 370, 1450
Dietrich, T., Samajdar, A., Khan, S., et al. 2019, PhRv, D100, 044003
Drischler, C., Melendez, J., Furnstahl, R., & Phillips, D. 2020, PhRvC, 102, 054315
Epelbaum, E., Hammer, H.-W., & Meissner, U.-G. 2009, RvMP, 81, 1773

Epelbaum, E., Krebs, H., & Meißner, U.-G. 2015, EPJA, 51, 53
Essick, R., & Landry, P. 2020, ApJ, 904, 80
Essick, R., Landry, P., & Holz, D. E. 2020a, PhRvD, 101, 063007
Essick, R., Tews, I., Landry, P., Reddy, S., & Holz, D. E. 2020b, PhRvC, 102, 055803
Essick, R., Tews, I., Landry, P., & Schwenk, A. 2021, PhRvL, 127, 192701
Fonseca, E., et al. 2021, ApJ, 915, L12
Gezerlis, A., Tews, I., Epelbaum, E., et al. 2013, PhRvL, 111, 032501
Gezerlis, A., Tews, I., Epelbaum, E., et al. 2014, PhRvC, 90, 054323
Glendenning, N. K. 1992, PhRvD, 46, 1274
Greif, S., Raaijmakers, G., Hebeler, K., Schwenk, A., & Watts, A. 2019, MNRAS, 485, 5363
Heinzel, J., Coughlin, M. W., Dietrich, T., et al. 2021, MNRAS, 502, 3057
Hinderer, T., et al. 2019, PhRvD, 100, 06321
Huth, S., Wellenhofer, C., & Schwenk, A. 2021, PhRvC, 103, 025803
Jeffreys, H. 1961, Theory of Probability (3rd ed.; Oxford, England: Oxford)
Kalogera, V., & Baym, G. 1996, ApJL, 470, L61
Kasen, D., Metzger, B., Barnes, J., Quataert, E., & Ramirez-Ruiz, E. 2017, Natur, 551, 80
Kawaguchi, K., Shibata, M., & Tanaka, M. 2020, ApJ, 889, 171
Lattimer, J. M. 2012, ARNPS, 62, 485
Li, B.-A., Cai, B.-J., Xie, W.-J., & Zhang, N.-B. 2021, Univ, 7, 182
Lipunov, V. M., et al. 2017, ApJL, 850, L1
Lonardoni, D., Carlson, J., Gandolfi, S., et al. 2018, PhRvL, 120, 122502
Lynn, J. E., Tews, I., Carlson, J., et al. 2016, PhRvL, 116, 062501
Lynn, J. E., Tews, I., Gandolfi, S., & Lovato, A. 2019, ARNPS, 69, 279
Machleidt, R., & Entem, D. R. 2011, PhR, 503, 1
Margalit, B., & Metzger, B. D. 2017, ApJL, 850, L19
Metzger, B. D. 2017, arXiv:1710.05931
Miller, M., Lamb, F. K., Dittmann, A. J., et al. 2021a, NICER PSR J0740 +6620 Illinois-Maryland MCMC Samples, Zenodo doi:10.5281/zenodo.4670689
Miller, M. C., Chirenti, C., & Lamb, F. K. 2019a, ApJ, 888, 12
Miller, M. C., et al. 2019b, ApJL, 887, L24
Miller, M. C., et al. 2021b, ApJL, 918, L28
Most, E. R., Weih, L. R., Rezzolla, L., & Schaffner-Bielich, J. 2018, PhRvL, 120, 261103
NICER. 2021
Ozel, F., & Freire, P. 2016, ARA&A, 54, 401
Piarulli, M., et al. 2018, PhRvL, 120, 052503
Raaijmakers, G., Greif, S. K., Hebeler, K., et al. 2021, arXiv:2105.06981
Raaijmakers, G., et al. 2020, ApJL, 893, L21
Radice, D., Bernuzzi, S., Del Pozzo, W., Roberts, L. F., & Ott, C. D. 2017, ApJ, 842, L10
Radice, D., & Dai, L. 2019, EPJ, A55, 50
Radice, D., Perego, A., Zappa, F., & Bernuzzi, S. 2018, ApJ, 852, L29
Rezzolla, L., Most, E. R., & Weih, L. R. 2018, ApJ, 852, L25
Riley, T. E., Watts, A. L., Ray, P. S., et al. 2021b, A NICER View of the Massive Pulsar PSR J0740+6620 Informed by Radio Timing and XMM-Newton Spectroscopy: Nested Samples for Millisecond Pulsar Parameter Estimation, v.v1.0.0, Zenodo doi:10.5281/zenodo.4697625
Riley, T. E., et al. 2019, ApJL, 887, L21
Riley, T. E., et al. 2021a, ApJL, 918, L27
Ruiz, M., Shapiro, S. L., & Tsokaros, A. 2018, PhRv, D97, 021501
Soares-Santos, M., et al. 2017, ApJ, 848, L16
Somasundaram, R., & Margueron, J. 2021, arXiv:2104.13612
Struder, L., et al. 2001, A&A, 365, L18
Tanvir, N. R., et al. 2017, ApJ, 848, L27
Tews, I., Carlson, J., Gandolfi, S., & Reddy, S. 2018a, ApJ, 860, 149
Tews, I., Gandolfi, S., Gezerlis, A., & Schwenk, A. 2016, PhRvC, 93, 024305
Tews, I., Margueron, J., & Reddy, S. 2018b, PhRv, C98, 045804
Tews, I., Pang, P. T. H., Dietrich, T., et al. 2021, ApJL, 908, L1
Turner, M. J. L., et al. 2001, A&A, 365, L27
Valenti, S., Sand, D. J., Yang, S., et al. 2017, ApJ, 848, L24
Wolff, M. T., et al. 2021, ApJL, 918, L26